Accepted Manuscript

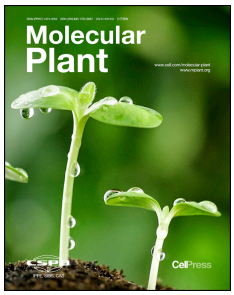

ESCRT-I component VPS23A affects ABA signaling by recognizing ABA receptors for endosomal degradation

Feifei Yu, Lijuan Lou, Miaomiao Tian, Qingliang Li, Yanglin Ding, Xiaoqiang Cao, Yaorong Wu, Borja Belda-Palazon, Pedro L. Rodriguez, Shuhua Yang, Qi Xie

PII: S1674-2052(16)30271-4
DOI: 10.1016/j.molp.2016.11.002
Reference: MOLP 389

To appear in: *MOLECULAR PLANT*
Accepted Date: 5 November 2016

Please cite this article as: **Yu F., Lou L., Tian M., Li Q., Ding Y., Cao X., Wu Y., Belda-Palazon B., Rodriguez P.L., Yang S., and Xie Q.** (2016). ESCRT-I component VPS23A affects ABA signaling by recognizing ABA receptors for endosomal degradation. Mol. Plant. doi: 10.1016/j.molp.2016.11.002.

ESCRT-I component VPS23A affects ABA signaling by recognizing ABA receptors for endosomal degradation

Feifei Yu[1,2], Lijuan Lou[1], Miaomiao Tian[1], Qingliang Li[1], Yanglin Ding[3], Xiaoqiang Cao[1], Yaorong Wu[1], Borja Belda-Palazon[4], Pedro L. Rodriguez[4], Shuhua Yang [3] and Qi Xie [1,*]

[1]State Key Laboratory of Plant Genomics, National Center for Plant Gene Research, Institute of Genetics and Developmental Biology, Chinese Academy of Sciences, Chaoyang District, Beijing, 100101, P. R. China

[2]University of Chinese Academy of Sciences, Beijing, 100049, P. R. China

[3]State Key Laboratory of Plant Physiology and Biochemistry, College of Biological Sciences, China Agricultural University, Beijing 100193, China

[4]Instituto de Biología Molecular y Celular de Plantas, Consejo Superior de Investigaciones Científicas-Universidad Politécnica de Valencia, 46022 Valencia, Spain

[*]Correspondence: qxie@genetics.ac.cn

Short Summary: The reverse-genetic screening of various *E2* or *UEV* mutant lines in response to ABA treatment identified E2-like VPS23A as an ABA negative regulator. The ESCRT-I component VPS23A affects PYR1/PYL4 via vacuole-mediated degradation besides 26S proteasome system, which strengthens our understanding of both the turnover of ABA receptors and ESCRTs in plant hormone signaling.

ABSTRACT

The recent discovery of PYR/PYL/RCAR-type ABA receptors has been one of most significant advances in plant science. In mammals, endosome sorting acts as an important pathway to down-regulate different types of receptors, but this kind of regulation of hormone signaling is poorly understood in plants. Here, we report that an ubiquitin E2-like protein, VPS23A, also a key component of ESCRT-I, negatively regulates ABA signaling. *VPS23A* has epistatic relation with *PYR/PYL/RCAR* type ABA receptors and deletion of *VPS23A* enhances the activity of key kinase OST1 in ABA signaling pathway under ABA treatment. Moreover, VPS23A interacts with PYR1/PYLs and K63-linked diubiquitin, and PYL4 possesses K63-linked ubiquitinated modification *in vivo*. VPS23A affects the subcellular localization of PYR1 and stability of the PYL4 by *vps23a* mutant analysis. These findings supports that VPS23A affects PYR1/PYL4 via vacuole-mediated degradation besides 26S proteasome system, further strengthen our understanding of both the turnover of ABA receptors and ESCRTs in plant hormone signaling.

Key words: ABA receptors, ESCRTs, ubiquitin, endosomal trafficking

Running title: VPS23A affects ABA receptors by endocytosis

INTRODUCTION

Abscisic acid (ABA) perception was difficult to study before the exclusively recognized pyrabactin resistance (PYR)/PYR1-like (PYL)/regulatory components of the ABA receptor (RCAR) family, which includes 14 members (PYR1, PYL1-13/RCAR1-14) in Arabidopsis, (Ma et al., 2009; Park et al., 2009) were identified. The refined ABA signaling cascade (in which PYR/PYL/RCAR ABA receptors perceive the primary ABA signal) comprises type 2C protein phosphatases (PP2Cs), SNF1-related protein kinase 2 (SnRK2s) and a series of substrates of SnRK2s, such as the bZIP transcription factor ABA-insensitive5 (ABI5), and the membrane ion channel protein slow anion channel-associated1 (SLAC1) (Yu et al., 2016). The transcriptional regulation of downstream regulators of ABA signaling is sophisticatedly regulated. For example, *ABI5* transcriptional expression can also be regulated by the AP2 domain transcription factor ABI4, which binds to the *ABI5* upstream regulatory region (Bossi et al., 2009).

Recently, the regulatory role of ubiquitination in ABA signaling has been extensively studied (Yu et al., 2015; Yu et al., 2016), especially the subtle modulation of PYR/PYL/RCAR-type ABA receptors by ubiquitination-mediated degradation via the 26S proteasome. PYR/PYL/RCAR-type ABA receptors were first reported as soluble proteins located between the cytosol and nucleus, and most of these proteins function redundantly, with the exception of PYL8 (Antoni et al., 2013). PYL8 interacts with the substrate receptor deetiolated1 (DET1)-, damaged DNA binding protein1 (DDB1)-associated1 (DDA1) in the nucleus (Irigoyen et al., 2014). DDA1 is responsible for the substrate specificity of cullin4-RING E3 ubiquitin ligases (CRL4s) by recognizing and thus accelerating the protein degradation of PYL8 via the ubiquitin proteasome system (UPS), contrary to the effect of ABA (Irigoyen et al., 2014). Unlike DDA1, the single unit RING-type E3 ligase, ring finger of seed longevity1 (RSL1), can interact with PYL4 and RSL1 on the plasma membrane, thereby promoting the ubiquitination and degradation of PYR1 and PYL4 (Bueso et al., 2014). The specific C2-domain ABA-related (CAR) signature of CAR4 is likely responsible for the recruitment of ABA receptors to the plasma membrane (Rodriguez et al., 2014).

Ubiquitinated membrane receptor can be recognized and transported through the

endosomal sorting complex and is required for the transport (ESCRTs) machinery that includes ESCRT-0, ESCRT-I, ESCRT-II and ESCRT-III complexes and is subsequently sequestered into vacuoles/lysosomes for degradation by luminal proteases (Henne et al., 2013; Shields and Piper, 2011). Although homologs of most ESCRT 0-III complex components occurring in yeast and mammals are found in the Arabidopsis genome (Barberon et al., 2014; Hurley and Emr, 2006), the functions of only a few of these homologs have been explored. Among these homologs, Arabidopsis FYVE1, which has been predicted to act as a subunit of ESCRT-I (a PI3P-binding protein that is located on late endosomes), is the most studied (Barberon et al., 2014; Hurley and Emr, 2006; Gao et al., 2014; Gao et al., 2015). FYVE1, also termed FREE1 (FYVE domain protein required for endosomal sorting 1), is essential for plant growth due to its role in MVB (Multivesicular Bodies) biogenesis and membrane-protein sorting in cells (Gao et al., 2014). FYVE1 acts as a crucial modulator of iron-regulated transporter1 (IRT1)-dependent metal transport and metal homeostasis by regulating the endosomal recycling of IRT1 back to the plasma membrane (Barberon et al., 2014). Additionally, a study of FREE1 implied the possibility of crosstalk between the ESCRT machinery and autophagy (Gao et al., 2015).

Arabidopsis ELC (also termed VPS23A) is a homolog of yeast VPS23p and human tumor susceptibility gene101 (TSG101), which are components of ESCRT-I. Both yeast Vps23p and human TSG101 are required for the efficient trafficking and degradation of misfolded cell-surface receptors (Babst et al., 2000). Vps23p, which has been identified as one of the suppressors of temperature-sensitive α-factor receptor (mutation *ste2-3*) and arginine permease (mutation *can1*^{ts}), plays no obvious role in cell division, whereas human TSG101 has been implicated in several biological processes, including cytokinesis, cell cycling and proliferation, protein ubiquitination, transcriptional regulation, and viral budding (Jiang et al., 2013; Li et al., 1999). Arabidopsis VPS23A was found to act in trichome morphogenesis and cytokinesis (Spitzer et al., 2006), but the molecular mechanism remains poorly understood. VPS23A possesses a ubiquitin-conjugating enzyme variant (UEV) domain that lacks the functional cysteine that is conserved in ubiquitin-conjugating (UBC) domains, which suggests that it can bind ubiquitin (Spitzer et al., 2006). Given the critical role of monoubiquitination (single or multiple) or K63-linked polyubiquitination in cargo reorganization and sorting

(Mukhopadhyay and Riezman, 2007; Traub and Lukacs, 2007), a functional analysis of VPS23A might effectively enhance our understanding of ECSRTs in the plant trafficking pathway. Here, VPS23A was found to be important in ABA signaling due to its interaction with ABA receptors. VPS23A and PYR1/PYL4 were co-localized on vesicle-like compartments, and the subcellular localization and stability of ABA receptors were affected in the *vps23a* mutant. All of the biochemical, cellular biological and genetic results obtained imply that VPS23A affects the ABA-signaling pathway and PYR1/PYLs stability via vacuole-mediated degradation.

RESULTS

vps23a mutant is sensitive to ABA

To uncover the role of UBC E2 or UEV E2-like in ABA signaling, a reverse-genetics approach was applied to screen various E2 or UEV mutant lines in response to ABA treatment. Among the tested mutant lines, a *vps23a* mutant (CS878714) in the *VPS23A* gene showed an ABA-hypersensitive phenotype in terms of cotyledon greening, and this line was chosen for further study. Detailed analysis showed that cotyledon greening and root growth were severely inhibited in the *vps23a* mutant compared with Col-0 under ABA treatment (Figure 1A and 1B). In the presence of 0.3 μM ABA, less than 10% of the mutant plants possessed expanded and green cotyledons, whereas 80% of Col-0 plants showed this phenotype (Figure S1B); the primary root length of the mutant was 50% less than that of the wild-type (Figure 1A and 1B). A dosage-dependent phenotype was observed, and under 0.5 μM ABA treatment, a more severe phenotype was observed (Figure 1). At the germination stage, there was no obvious difference between the *vps23a* mutant and Col-0 in terms of ABA response (Figure S1C-S1E), which implies that VPS23A mainly acts on ABA signaling at the post-germination stage. Two randomly selected *vps23a* complementary plants, P_{VPS23A}-*VPS23A* (*vps23a*) lines 3.3 and 4.6, complemented the ABA-sensitive phenotype, thus verifying that the phenotype of *vps23a* is indeed due to the *VPS23A* gene knockout. Additionally, as shown in Figure S1F and G, *vps23a* showed a sensitive phenotype at the post-germination stage in terms of both aerial part and root growth, and complementation lines almost fully rescued the sensitive

phenotypes. Together, these findings show that VPS23A is involved in the ABA pathway, and the dose-dependence of the phenotype indicates that VPS23A affects signaling transduction rather than the ABA metabolic pathway.

OST1 activity and ABA-responsive gene expression are elevated in the *vps23a* mutant

Plants receive ABA signals through PYR/PYL/RCAR-type ABA receptors and promote SnRK2s to positively act in signal transduction (Raghavendra et al., 2010). Open stomata 1 (OST1) is a member of the SnRK2 family and can phosphorylate ABRE-binding proteins/factors (AREBs/ABFs) to regulate the expression of stress-responsive genes in ABA signaling, for example, the bZIP transcription factor ABI5 (Furihata et al., 2006; Mustilli et al., 2002; Ding et al., 2015). An in-gel protein kinase assay showed that OST1 activity was hardly detected without ABA treatment, and induced by ABA treatment for 30 min in both Col-0 and *vps23a* mutant (Figure 2A). Under ABA treatment, although the total loading proteins of *vps23a* is less than Col-0 as indicated by Ponceau S-stained ribulose-1,5-bisphosphate carboxylase/oxygenase (Rubisco), the phosphorylated signal indicative of OST1 activity is higher with *vps23a* than with Col-0 (Figure 2A), suggesting that VPS23A might act in the ABA signaling that is perceived by members of the PYR/PYL/RCAR family. A qRT-PCR assay showed that the expression levels of *ABI4* and *ABI5* were approximately 2- to 3-fold higher in the *vps23a* than those in WT plants when germinated on a medium that was supplemented with 0.5 μM ABA (Figure 2B and 2C). Consistently, ABI5 protein levels were significantly higher in *vps23a* than in WT when supplemented with 0.5 μM ABA or 100 mM NaCl, (Figure 2D). These data indicate that VPS23A regulates key regulators upstream of OST1 and then affects the expression of key transcriptional factors at both the transcriptional and translational levels to activate ABA signaling.

***PYR/PYL/RCAR* ABA receptors acts in a genetically epistatic manner to *VPS23A* during ABA signaling**

To analyze the genetic relationships between *VPS23A* and key factors in ABA signaling, genetic crosses between *vps23a* and mutants of key components of the ABA-signaling pathway were performed, and the resulting phenotypes were analyzed. Consistent with the

altered expression of *ABI4* and *ABI5* in the *vps23a* mutant (Figure 2B and 2C), the double mutants *vps23a abi4-T* and *vps23a abi5-1* showed similar ABA-insensitive phenotypes with *abi4-T* and *abi5-1*, in contrast to the ABA-sensitive phenotype of *vps23a* (Figure 3A, Figure S2A and S2B). Thus, the genetic evidence suggests that both *ABI4* and *ABI5* act downstream of *VPS23A* in the ABA pathway.

Given the higher OST1 activity in the *vps23a* mutant compared to Col-0 (Figure 2A), *VPS23A* might act upstream of *SnRK2s* in the ABA pathway. The co-receptor ABA-insensitive1 (ABI1) is a member of the PP2C family, which negatively regulates OST1 in the ABA pathway (Furihata et al., 2006). The dominant mutant *abi1-1*, which contains a point mutant $ABI1^{G180D}$ that cannot interact with PYR1, exhibited an ABA-insensitive phenotype during cotyledon greening (Armstrong et al., 1995). The double mutant *vps23a abi1-1* exhibited an ABA-insensitive phenotype similar to that of *abi1-1*, suggesting that *abi1-1* can rescue the ABA-sensitive phenotype of *vps23a* (Figure 3B and Figure S2C). The data imply that *VPS23A* also acts upstream of *ABI1*. *abi1-2* is a loss-of-function mutant of ABI1, and *hab1-1* is the mutant in hypersensitive to ABA1 (HAB1), another PP2C that cooperates with ABI1 to negatively regulate ABA signaling (Saez et al., 2006). The double mutant *abi1-2 hab1-1* exhibited strong hypersensitivity to ABA (Saez et al., 2006). Interestingly, the triple mutant *vps23a abi1-2 hab1-1* exhibited a more ABA-hypersensitive phenotype than the single mutant *vps23a* or the double mutant *abi1-2 hab1-1* (Figures S2C and S2E), implying that VPS23A might directly or indirectly affect ABI1 and HAB1.

pyr1 pyl1 pyl2 pyl4 was less sensitive to ABA-mediated seedling establishment than Ler and Col-0 (Park et al., 2009), opposite to the *vps23a* mutant. *pyr1 pyl1 pyl2 pyl4* partially rescued the sensitive phenotype of *vps23a* in terms of seedling establishment and root growth on medium supplemented with various concentrations of ABA (Figures 3B, S2D and S3A and S3B). Statistical analysis of cotyledon greening showed that almost no cotyledons of *vps23a* plants became green within one week on medium supplemented with 0.3 μM ABA, whereas approximately 30% of Col-0, 50% of Ler and *pyr1 pyl1 pyl2 pyl4 vps23a*, and 100% of *pyr1 pyl1 pyl2 pyl4* plant cotyledons turned green (Figure S2D). A seedling transfer assay showed similar ABA phenotypes (Figure S3A and S3B). However, phosphorylation signals were not detected in samples of *pyr1 pyl1 pyl2 pyl4 vps23a* because the quintuple mutant exhibited the

same OST1 activity defect as the quadruple mutant *pyr1 pyl1 pyl2 pyl4*. OST1 activity also matched the phenotype of the quintuple mutant (Figure S3C). Taken together, these findings indicate that VPS23A likely functions with PYR/PYL/RCAR ABA receptors in the ABA perception pathway and may be epistatic with these receptors.

VPS23A and PYR1/PYL4 co-localize in endosomal compartments

Transient co-expression of GFP-VPS23A with the early endosome (EE) marker SCAMP1-RFP, the *trans*-Golgi network (TGN) marker MANI-RFP and the late endosome (LE) marker ARA7-RFP (Figure 4A) verified that VPS23A is localized in the endosomal compartment (Spitzer et al., 2006). In a recent work describing the role of membrane RING E3 ligase RSL1 in the ABA-signaling pathway, the authors speculated that ubiquitinated PYLs might be sorted into vacuoles for degradation (Bueso et al., 2014). PYR1 and PYL4 partially localized with the early endosome and TGN, directly supporting the possible recycling of ABA receptors through the endocytic pathway because the trans-Golgi network acts as an early endosome in plants (Valencia et al., 2016) (Figure 4B). Wortmannin (WM) specially inhibits phosphatidylinositol 3 (PI3) kinase activity, resulting in the blockade of protein cargo trafficking to vacuoles and the formation of enlarged multivesicular bodies (MVBs) (Robinson et al., 2008). Under WM treatment, PYR1/PYL4-GFP displayed more punctate dots and merged very well with the late endosomal marker ARA7-RFP compared with the situation without WM treatment, further suggesting that PYR1/PYL4 is indeed affected by the endocytic pathway (Figure 4C). Logically, mCherry-VPS23A co-localized with PYR1/PYL4-GFP on the intracellular vesicles, as further verified by live-cell time-lapse imaging of their co-localization on the mobile vesicle or endosome (Figure 4D). Thus, these results demonstrate the membrane localization of PYR1/PYL4 and their endosomal localization and movement with VPS23A in the endosome compartment.

PYR/PYL/RCAR ABA receptors interact with VPS23A and other components of ESCRT-I

The co-localization of VPS23A with PYL4 indicated the possibility that they might interact. Members of the VPS23 family are known to directly interact with their substrate protein for

sorting. Co-immunoprecipitation (Co-IP) assays and firefly luciferase complementation imaging (LCI) assays proved that VPS23A and PYL4 interact *in vitro* and *in vivo* (Figure 5A and 5B). In fact, VPS23A can interact with all fourteen members of the PYR/PYL/RCAR family (Figure S4A). Because the UEV domain of VPS23A was responsible for binding ubiquitin molecules (Spitzer et al., 2006), we then examined the interaction between VPS23A and PYL4. A pull-down assay of GST or GST-VPS23A with PYL4-Nluc, as expressed in plants, demonstrated that only GST-VPS23A can precipitate the PYL4-Nluc protein at predicted unmodified size, and perhaps ubiquitinated, especially the K63-linked ubiquitinated proteins (Figure 5C). Similarly, the pull-down assay of GST or GST-VPS23A with PYL1-Nluc also showed that VPS23A can precipitate the ubiquitinated form of PYL1 as shown in Figure S4B. To verify VPS23A not only recognizes PYL4 proteins themselves but also the K63-linked ubiquitin chains, another pull-down assay with GST-VPS23A and K63-linked diubiquitin were performed. As shown in Figure 5D, the result demonstrated that VPS23A can also recognize the K63-linked diubiquitin. Considering these findings together, we concluded that VPS23A probably recognizes both non-ubiquitinated and ubiquitinated PLYs in plants.

It has been reported that VPS23A interacts with Arabidopsis homologs of the ESCRT-I complex (Spitzer et al., 2006). Taking into account the interaction between VPS23A and PYL4, the relationship between PYL4 and other members of the ESCRT-I complex, including VPS23B, VPS28-1, VPS28-2, VPS37-1 and VPS38-2, was explored. PYL4 was confirmed to interact with those ESCRT-I components by LCI assay, as shown in Figure S4C. PYR1 also interacts with ESCRT-I components (Figure S4D). These results indicate that at least some portion of PYL4/PYR1 may be collected by protein sorting process that is mediated by ESCRT complexes.

VPS23A affects the vacuolar biogenesis and subcellular localization of PYR1

FREE1 was recently discovered to be a new component of ESCRT-I and to regulate the formation of the central large vacuole (Gao et al., 2015). Because VPS23A is a key component of ESCRT-I (Spitzer et al., 2006), we then checked whether VPS23A can also affect the formation of vacuoles. A 2',7'-bis-(2-carboxyethyl)-5-(and-6)-carboxy

fluorescein)-acetoxymethyl ester (BCECF-AM) probe that labels acidic compartments, such as vacuoles, was used to stain the vacuoles of Col-0 and the *vps23a* mutant. The results showed that the *vps23a* mutant exhibits abnormal vacuole morphology (Figure 6A). To analyze the vacuolar structure in greater detail, 3D reconstruction analysis of the stained cells of both Col-0 and the *vps23a* mutant was performed by surface rendering on Z-stack images (Figure 6A). The abnormal vacuole morphology may be the reason of altered localization of PYR1 in the *vps23a* mutant.

To investigate the possible sorting role of VPS23A to PYR/PYL/RCAR-type ABA receptors, P_{PYR1}*-PYR1-GFP*::*vps23a* and P_{PYR1}*-PYR1-GFP*::Col-0 transgenic plants with similar transcriptional level of *PYR1* (Figure S4E) were generated to explore the role of VPS23A in PYR1 endosomal trafficking. T_2 transgenic plants were used in the assay. The plants with expression level of PYR1-GFP were used for assay. PYR1-GFP displayed cytosolic and nuclear localization in the root tips of the P_{PYR1}*-PYR1-GFP*::Col-0 transgenic line but was strongly localized in endocytic vesicles in the P_{PYR1}*-PYR1-GFP*::*vps23a* plants; this accumulation pattern is shown merged with the staining of FM4-64 in Figure 6B. This result indicates that the deletion of VPS23A can affect the subcellular localization of PYR1 and might affect the protein status of PYR1 through the endocytic pathway via the lytic vacuole.

VPS23A affects the protein stability of PYL4

ESCRTs play important roles in trafficking ubiquitinated cargo into the intraluminal vesicles (ILVs) of prevacuolar compartments (PVCs)/MVBs, and the ubiquitinated cargo is then delivered into vacuoles/lysosomes for degradation. To investigate the effect of PYL protein stability on the vacuole/lysosome degradation pathway, 10-day-old transgenic plants of HA-PYL4, with and without E64D (an inhibitor of lysosomal/vacuolar hydrolases) treatment, were used in the assay. HA-PYL4 degraded rapidly under cycloheximide (CHX, an efficient inhibitor of eukaryotic protein synthesis) chase treatment, indicating that PYL4 is an unstable protein (Bueso et al., 2014). When E64D was added, the degradation of HA-PYL4 slowed compared to the control treatment. For instance, HA-PYL4 was not detected after 6 h of CHX treatment but was still detectable in CHX- and E64D-treated samples (Figure 7A; Figure

S5A). These data suggest that PYL4 degradation may be partially mediated by the vacuole/lysosome pathway.

Given the role of ESCRTs in vacuole-mediated degradation, we speculated that VPS23A should affect the protein stability of PYL4. An *in vivo* co-expression assay showed that the PYL4-Nluc protein level was evidently decreased when co-expressed with GFP-VPS23A *in planta* compared to GFP, a finding that supported the above speculation (Figure 7B; Figure S5B). To quantitatively measure the effect of VPS23A on PYL4, different amounts of GFP-VPS23A were mixed with equal amounts of PYL4-Nluc protein, both expressed *in planta*. As shown in Figure 7C and Figure S5C, PYL4-Nluc levels were markedly decreased as the amount of GFP-VPS23A increased. These results suggest that VPS23A can accelerate the protein degradation of PYL4. VPS23A-dependent PYL4 proteolysis was also observed in Arabidopsis, and the half-life of HA-PYL4 was investigated in the *vps23a* mutant and the wild-type. As shown in Figure 7D and Figure S5D, under standard growth conditions, HA-PYL4 was slightly accumulated in the *vps23a* mutant compared with the WT. The time-course assay also indicated that HA-PYL4 degraded more rapidly in Col-0 than in the *vps23a* mutant under CHX treatment. The PYL4 antibody was obtained, and was used to detect the accumulation of endogenic PYL4 in Col-0 and *vps23a* with or without ABA treatment. As shown in Figure 7E, the protein levels of PYL4 have no much difference between Col-0 and *vps23a* without ABA, while PYL4 accumulates more in *vps23a* than Col-0 under ABA treatment, suggesting the protein stability of PYL4 can be affected by VPS23A *in vivo* under ABA treatment condition. Similar results were obtained for PYR1 and PYL8 (Figure S5E-S5H). Considering the above findings together, we conclude that VPS23A can indeed affect the degradation of PYL4 via the lysosome/vacuole-mediated pathway.

VPS23A affects ubiquitin conjugates, and K63-linked polyubiquitin chains of PYL4 are presented in Arabidopsis

A previous study indicated that VPS23A can bind ubiquitin or ubiquitinated proteins (Spitzer et al., 2006); therefore, the question of whether the abnormal vacuolar structure of *vps23a* (Figure 6A) can affect the ubiquitin cargo to be sorted into the vacuole for degradation was explored. As shown in Figure S6A, higher levels of ubiquitinated conjugates were present in

vps23a than in Col-0, especially in ABA-treated samples, implying that VPS23A functions in the removal of ubiquitinated proteins, similar to the function of ALIX and FREE1 (Gao et al., 2014; Kalinowska et al., 2015).

ESCRTs are engaged in the process by which ubiquitination directs internalized proteins toward lysosomal degradation (Clague and Urbe, 2006). PYL4 ubiquitination was detected *in vivo* and was proven to be catalyzed by the E3 ligase, RSL1 (Bueso et al., 2014). However, the form adopted by the ubiquitin chains of PYL4 has not been reported. Mono-ubiquitination is essential for initial internalization, but efficient protein sorting in the endosomal system by the ESCRT complexes requires K63-linked poly-ubiquitin (Lauwers and Andre, 2009). When probed with the antibody P4D1, which recognizes both poly- and mono-ubiquitinated proteins, a high-molecular-weight smear was observed, representing ubiquitinated HA-PYL4; the same result was obtained using the FK1 antibody, which recognizes only poly-ubiquitinated proteins (Figure S6B). These findings suggest the existence of a poly-ubiquitinated form of PYL4 but do not exclude or confirm the presence of mono-ubiquitinated forms. Intriguingly, both K48- and K63-linked poly-ubiquitin chains were present in the HA-PYL4 precipitates, as verified by the use of chain-specific ubiquitin antibodies (Figure S6B); this indicates that the degradation of PYL4 occurs via both the 26S proteasome and the lysosome/vacuole pathway. Collectively, the obtained data verified the K63-linked poly-ubiquitin modification of PYL4 and the interaction of K63-linked diubiquitin with VPS23A, thus supporting the idea that the stability of PYL4 can indeed be regulated by lysosomal/vacuolar degradation via an interaction with ESCRT components.

DISCUSSION

In this study, we discovered that the *vps23a* mutant (containing a deletion of the ESCRT-I component, VPS23A) was sensitive to ABA treatment by screening T-DNA-inserted mutants of E2 or E2-like coding genes. The higher activity of OST1 kinase in *vps23a* strongly suggested that VPS23A plays a crucial role in the ABA pathway that is initiated by PYR/PYL/RCAR-type ABA receptors, which bind ABA and inhibit PP2C phosphatases, thus releasing the inhibition of OST1 by PP2C (Hao et al., 2011; Vlad et al., 2009; Ma et al., 2009;

Park et al., 2009). Thus, VPS23A should be a negative regulator in ABA signaling. This is the first report of a component of the ESCRT-I complex participating in the ABA response in plants. In the Arabidopsis genome, there is another copy of VPS23, VPS23B; unfortunately, no mutant was identified for VPS23B. Thus, we were unable to conclude whether VPS23B is also involved in negatively regulating ABA signaling; if so, double mutants should show more sensitivity to ABA. The ESCRT-III-related protein lyst-interacting protein5 (LIP5) strongly interacts with suppressor of K^+ transport growth defect1 (SKD1) AAA ATPase, which is essential for ESCRT-III disassembly (Haas et al., 2007; Scott et al., 2005). Xia et al. found that LIP5 knockdown mutants had ABA-insensitive phenotypes and exhibited reduced drought tolerance; suggesting that LIP5 positively regulates drought tolerance through ABA-mediated cell signaling (Xia et al., 2016). The target of LIP5 or LIP5/SKD1 in the ABA pathway has not been found, and if PYLs are targets, then the effect of ESCRT-III disassembly on the ABA receptor requires study. LIP5 deletion results in compromised tolerance to both heat and salt stresses compared to the wide-type. Higher amounts of cellular NaCl but reduced levels of reactive oxygen species (ROS) in cells may explain the reduced salt tolerance exhibited by the *lip5* mutant (Wang et al., 2015). These studies collectively provide insight into the potential roles of ECSRTs in phytohormone ABA signaling and abiotic responses.

The genetic evidence obtained indicated that VPS23A acts epistatically to the ABA co-receptor ABI1, a PP2C phosphatase, and to PYR/PYL/RCAR-type ABA receptors. In accordance with the role of VPS23A as a member of ESCRT-I, which is essential for the initial step (recognition) of sorting proteins (Bilodeau et al., 2002; Bilodeau et al., 2003), VPS23A disruption disturbs the subcellular localization of PYR1-GFP. Previously, PYR/PYL/RCAR-type ABA receptors were primarily identified as localized in the cytosol and nucleus (Ma et al., 2009; Park et al., 2009). We found that PYR1/PYL4-GFP also co-localizes with VPS23A/ELC in endocytotic compartments, similar with the co-localization pattern observed between PYL4 and its RING-type E3 ligase, RSL1 (Bueso et al., 2014). Small vesicles containing fluorescent signal in or near the plasma membrane were generated by the interaction between RSL1 and PYL4 under BFA treatment, thus emphasizing the vital role of RSL1 in PYL4 protein trafficking in cells (Bueso et al., 2014). Further protein

fractionation and biochemistry assays confirmed that a significant fraction of total PYL4 proteins were indeed localized in microsomes (Bueso et al., 2014). Thus, these lines of evidence all indicate that in addition to the cytosol and nucleus, PYR1/PYL4 are partially localized in endosomal compartments and are thus affected by VPS23A.

In yeast and mammals, both Vps27p/Hrs and Hse1p/STAM contain ubiquitin-interacting motifs (UIMs) that bind ubiquitin and recognize ubiquitinated cargo (Bilodeau et al., 2002). The UEV domain of Vps23p/TSG101 can interact simultaneously with ubiquitin and the P(S/T)xP motif of Vps27p/Hrs (Bilodeau et al.,2003; Katzmann et al., 2003; Lu et al., 2003). Previous research found that VPS23A can bind ubiquitin (Spitzer et al., 2006). We found that VPS23A can not only interact with the K63-linked diubiquitin but also endocytic cargo PYL4 protein itself. There are two possibilities: (i) The cargoes may be recruited by FREE1/FYVE1 (Belda-Palazon et al., 2016), and then delivered to VPS23A through their mutual interaction, or the UEV domain of VPS23A can accept the K63-linked ubiquitin chains of the cargoes, which is supported by the co-localization of FREE1 and VPS23A on LE/MVB (Belda-Palazon et al., 2016); (ii) VPS23A can directly recognize and recruit non-ubiquitinated or K63-lined ubiquitinated endocytic cargoes independently of the unidentified ECSRT-0 complex. Upon to now, there are very few works about K63-linked ubiquitinated modifications of endocytotic cargo in plants, including the auxin carrier protein PIN2 and brassinosteroid receptor kinase BR insensitive1 (BRI1) (Leitner et al., 2012; Martins et al., 2015). Collectively, in some cases, the recognition of PYL4 by the endosomal trafficking pathway might depend on a direct interaction with the sorting complexes; in other cases, this recognition might rely on post-translational modifications, such as ubiquitination or phosphorylation (Reyes et al., 2011).

Known targets of the endocytic trafficking route in plants include the auxin carriers PIN1, PIN2, and AUX1, the iron transporter IRT1, the boric acid/borate exporter BOR1, the flagellin receptor FLS2, the brassinosteroid receptor BRI1, and the high-affinity phosphate transporter PHT1 (Barberon et al., 2011; Bayle et al., 2011; Geldner et al., 2001; Kasai et al., 2011; Kleine-Vehn et al., 2006; Kleine-Vehn et al., 2008; Spallek et al., 2013; Spitzer, et al., 2009). Most of these endosomal sorting cargoes are recognized and trafficked into lytic vacuoles and degraded in response to various signals. ESCRTs are integral to the degradation of

internalized membrane proteins (Slagsvold et al., 2006). PYR/PYL/RCAR receptors interact with ABI1 in different locations in the cell, similar to ABI1; despite not containing transmembrane domains, they have also been found partially associated with membrane. This type of association might be due to their modification by ubiquitin or association with other proteins, such as CAR4 (Rodriguez et al., 2014). A mutation of VPS23A, the key component of the ESCRT-I complex, exhibited slowed PYL4 degradation *in vivo,* indicating that PYL4 is a target in the ESCRT-mediated degradation pathway. PYL4 degradation can be alleviated by E64D, an inhibitor of lysosomal/vacuolar hydrolases (Bassham, 2007), as further confirmed by the K63-linked ubiquitin chain modification of PYL4. Previous studies showed that PYL4 is a degradative protein (Bueso et al., 2014) and that the degradation is mediated by the 26S proteasome, which recognizes substrates with K48-linked ubiquitin chains (Tomanov et al., 2014); these findings indicate the subtle regulation of PYR/PYL/RCAR-type ABA receptor ubiquitination in cells, which occurs in various cell compartments. It is noteworthy that the storage function of the endosomal sorting pathway via vacuoles cannot be excluded when considering the regulation of PYR/PYL/RCAR-type ABA receptors.

Taken together, these findings indicate that VPS23A probably affects ABA signaling and the degradation of PYR/PYL/RCAR-type ABA receptors via the endocytic pathway. It was interesting to find that small, soluble ABA receptors were recruited into the endosomal vesicle by VPS23A. This study will enhance our knowledge based on the findings that the K63-linked ubiquitin chain (the second-most abundant ubiquitin chain) and the interaction between ABA receptors PYR/PYLs with ESCRT-I complex also play important roles in controlling the activity of PYLs, supported by a very recent work found that FYVE1, another ESCRT-I component, recruits PYL4 into endosomal compartments to regulate turnover of PYL4 (Belda-Palazon et al., 2016). However, some questions remain unresolved. For example, both FYVE1 and VPS23A were found to bind ubiquitinated proteins and they can interact with each other (Gao et al., 2014). So whether FYVE1 and VPS23A cooperate to recognize cargo proteins needs further study. Also there are two homologs of mammalian Vps23/TSG101 in Arabidopsis (VPS23A and VPS23B); thus, the possibility of functional redundancy in the ABA response or other biological processes remains to be explored. Further studies on other ESCRT components involved in the ABA response and the response of

VPS23A to biotic and abiotic stresses should be explored.

METHODS

Plant materials and growth conditions

The *Arabidopsis thaliana* ecotypes Col-0, Ws-2 and Ler-0 were utilized in this study. The mutant line *vps23a* (CS878714) was purchased from ABRC (The Ohio State University, Columbus, OH, USA). To confirm and identify the homozygous mutant lines including *vps23a* (CS878714) and *abi4-T* (SALK_080095) with Col-0 backgrounds, *abi5-1* (CS8105) with Ws-2 background, *abi1-1* (CS22) with Ler-0 background and *pyr1 pyl1/2/4*, DNA was extracted from each mutant line individually and was subjected into genotyping by PCR assay with the primers listed in Table S1. The genetic mutant materials including *vps23a abi4-T*, *vps23a abi5-1*, *abi1-1 vps23a*, *vps23a abi1-2 hab1-1* and *pyr1 pyl1/2/4 vps23a* were generated by crossing *vps23a* with *abi4-T*, *abi5-1*, *abi1-1*, *abi1-2 hab1-1* and *pyr1 pyl1/2/4*, and homozygous F3 generation plants were used in the genetic analyses.

Seeds were surface-sterilized with 10% bleach and washed four times with sterile water. The sterile seeds were then plated on ½ MS medium with or without ABA and stratified at 4^{o}C for 3 d before transferring to a tissue culture room with long-day light conditions under a 16-h-light/8-h-dark photoperiod at 22^{o}C and 70% relative humidity. After a period between 7 and 14 d, the phenotypes were observed. To observe whole plant growth conditions, 3-day-old seedlings that were grown on ½ MS standard growth medium were transferred onto ½ MS medium containing ABA, and the phenotypes were observed.

Transformation vectors and constructs of transgenic plants

To investigate the co-localization of PYR1/PYL4 with various endosome-related markers, the coding regions of PYR1 and PYL4 fused to GFP at the C-terminal were cloned into pCambia1300-221 using the Quick-Fusion Cloning kit (Biotool) according to the manufacturer's instructions. Plasmid constructs of VPS23A with Myc, GFP and mCherry at the N-terminus were generated by cloning into pCambia1300-221 using the Quick-Fusion Cloning kit (Biotool) according to the manufacturer's instructions. Coding regions of

PYR1/PYL1-13 without stop codes and VPS23A were amplified by PCR using primers containing the appropriate restriction enzyme digestion sites and were cloned into pCambia1300-221-Nluc and pCambia1300-221-Cluc, respectively (Clough et al., 1998). GST-VPS23A was generated by cloning the coding region of VPS23A into the pGEX-6p-1 vector.

To produce a line complementary to the *vps23a* mutant, the coding sequences of *VPS23A* were fused with the native promoter of *VPS23A* using PCR; the resulting PCR fragment was cloned into the vector pCambia1300-221 including GFP at the N-terminal of *VPS23A* (P_{VPS23A}-*VPS23A*). This construct was introduced into the *A. tumefaciens* strain EHA105, and Arabidopsis transformation was performed using the floral dip method as described previously (Xie et al., 2002). T3 or T4 homozygous transgenic seeds were selected for phenotype analysis. The transgenic plants *PYR1-GFP*::Col-0 and *PYR1-GFP*::*vps23a* were generated using the floral dip method with the *A. tumefaciens* strain EHA105 containing *PYR1-GFP* constructs. T2 generation plants were used for subcellular localization analysis.

Protein kinase assay

The ABA-dependent phosphorylation activity of OST1 was analyzed using an in-gel kinase activity assay with GST-ΔABF2 as substrate according to a previously described method (Fujii et al., 2007) with some modifications. Total proteins were extracted from approximately 10-day-old seedlings under standard conditions or 30 min after 100 μM ABA treatment using protein extraction buffer (5 mM EDTA, 5 mM EGTA, 25 mM NaF, 20% glycerol, 1 mM Na_3VO_4, 5 mM DTT, 1 × protease inhibitor cocktail (Roche), 1 mM phenylmethyl sulfonylfluoride, and 50 mM HEPES-KOH, pH 7.5). The protein samples (40 mg/lane) were separated in an SDS-PAGE gel containing 0.5 mg/mL GST-ΔABF2 substrate peptide, which was expressed in *E. coli*. The gel was washed 3 × 20 min with 0.5 mg/mL BSA, 1 mM DTT, 5 mM NaF, 0.1 mM Na_3VO_4, 0.1% Triton X-100, and 25 mM Tris-HCl, pH 7.5, and proteins in the gel were renatured three times in 2 mM DTT, 5 mM NaF, 0.1 mM Na_3VO_4, and 25 mM Tris-HCl, pH 7.5, for 1 h, 12 h and 1 h at 4°C. After incubation with kinase reaction buffer (2 mM EGTA, 1 mM DTT, 0.1 mM Na_3VO_4, 12 mM $MgCl_2$, and 25 mM HEPES-KOH, pH 7.5) for 30 min at room temperature, the gel was immersed in 30 mL kinase reaction buffer

containing 60 μCi [γ-^{32}P]ATP and 9 μL cold ATP (1 mM) at room temperature for another 2 h. The SDS-PAGE gel was washed five times (30 min each time) with 5% TCA and 1% sodium pyrophosphate. Radioactivity was detected using a Typhoon 9410 imager.

RT-PCR and quantitative RT-PCR assay

Total RNA was extracted from 7-day-old seedlings of Col-0 and the *vps23a* mutant that were sown on ½ MS standard growth medium (either alone or supplemented with 0.5 μM ABA) using an Ultrapure RNA kit (CWBio) and was subjected to DNA removal and reverse transcription using a FastQuant RT kit with gDNase (TIANGEN). RT-PCR and qRT-PCR were performed using *ACTIN 1* and *ACTIN 7* as internal controls. Quantitative PCR was carried out using SsoFast EvaGreen Supermix (Bio-Rad) and a CFX96 Touch Real-Time PCR Detection System (Bio-Rad) as recommended by the manufacturer. The primers used for RT-PCR and qRT-PCR are listed in Table S1.

Transient expression assay in *N. benthamiana*

Agrobacterium-mediated transient expression in *N. benthamiana* was carried out according to a previously described protocol (Liu et al., 2010) with some modifications. Generally, when the OD_{600} of transformed *A. tumefaciens* strains EHA105 reached approximately 3.0, the bacteria were gently centrifuged (3500 g, 12 min), and the pellets were resuspended in 10 mM $MgCl_2$ to the appropriate concentration. Acetosyringone (final concentration, 200 μM) was added, and the bacteria were maintained at room temperature for 2 h before infiltration.

For the subcellular co-localization assay, the agrobacterium strains containing the various constructs and the gene-silencing suppressor P19 were first mixed to a final OD_{600}=0.5 or 0.33 accordingly, and the mixture was then co-infiltrated into tobacco leaves. After 2-3 days, fluorescence was detected using a Zeiss Axio Imager.z2. For the luciferase complementation image (LCI) assay, the tested genes were fused with Nluc at the C-terminus and Cluc at the N-terminus; then, the constructs were introduced into *A. tumefaciens* strains EHA105. Equal amounts of the two transformed bacteria were mixed with P19 and co-infiltrated into tobacco leaves for four days. LUC images were captured using a low-light cooled charge-coupled device imaging apparatus (NightOWL II LB983 with indiGO software). For the *in vitro*

degradation assay of PYR1/PYL4/PYL8, equal amounts of agrobacterium containing the different constructs (OD_{600}=1.5) were co-expressed with agrobacteria expressing P19 (OD_{600}=1.0) in tobacco leaves for three days; the samples were collected, quickly frozen in liquid nitrogen, and stored at -80^{o}C. For the *in vivo* degradation assay, an agrobacterial strain carrying constructs PYL4-Nluc and P19 were mixed with GFP-VPS23A or control GFP with RFP as an internal control, and mixtures with different ratios were co-infiltrated into tobacco leaves; leaves were harvested after 4 d for subsequent immunoblot analysis.

Drug and tracer treatments

For the WM treatment, tobacco leaves co-expressing PYR1/PYL4-GFP with ARA7-RFP were cut into small pieces and immersed into liquid ½ MS standard growth medium, which was or was not supplemented with 33 μM WM, for 30 min. To visualize vacuoles in root epidermis cells, 2-day-old seedlings of Col-0 and the *vps23a* mutant were exposed to 5 μM BCECF-AM, which was diluted in ½ MS standard medium; the stock was prepared by dissolving the substance in DMSO for 1 h in the dark. For FM4-64 staining, the seedlings were incubated with 2 μM FM4-64 for 30 min and then washed with ½ MS medium before visualization.

Microscopy

Confocal laser scanning microscopy was performed using a Zeiss Axio Imager.Z2 with excitation and detection wavelengths of 488 nm and 510-540 nm, respectively, for GFP and BCECF-AM; 561 nm and >575 nm, respectively, for RFP and mCherry; and 488 nm and >610 nm, respectively, for FM4-64. For 3D-reconstruction and surface rendering of the BCECF-AM stained vacuoles, from 70 to 100 Z-stack images were recorded (0.2 μm step size). The data were processed with Imaris 8 (Bitplane) with the parameters as follows: diameter of largest sphere, 1.00 μm; surface area detail level, 0.12 μm; background subtraction, enabled.

Pull-down and Co-IP assays

For the pull-down assay, the fusion GST-VPS23A protein was expressed in *E. coli* as described previously (Xie et al., 1999), and PYL4-Nluc was transiently expressed in tobacco

leaves. GST and GST-VPS23A proteins were purified with Glutathione SepharoseTM 4B beads (GE Healthcare). The PYL4-Nluc protein was extracted in native extraction buffer (0.5 M sucrose, 1 mM MgCl2, 10 mM EDTA, 50 mM Tris-MES pH 8.0, 5 mM DTT, protease inhibitor cocktail CompleteMini tablets (Roche), 1 mM phenylmethyl sulfonylfluoride, 0.4% NP40). Equimolar amounts of GST and GST-VPS23A proteins were incubated with equal amounts of PYL4-Nluc protein extracts at 4^{o}C for 2 h. After incubation, the beads containing GST and GST-VPS23A proteins were washed three times for 10 min each time; then, the eluted proteins were detected using anti-Luc, anti-Ub and anti-K63-Ub antibodies. For detection of the interaction between VPS23A with K63-Diub (BostonBiochem), equimolar amounts of GST and GST-VPS23A proteins were incubated with equal amounts of K63-Diub at 4^{o}C for 2 h. After incubation, the beads were washed three times; then, the eluted proteins were detected using anti-Ub antibody.

For the Co-IP assay, GFP, GFP-VPS23A and PYL4-Nluc proteins were transiently expressed, and samples were collected at appropriate times. The GFP and GFP-VPS23A samples were homogenized with native extraction buffer and incubated with beads that were coated with anti-GFP antibody for 2 h at 4^{o}C. After washing three times with PBS buffer pH 7.4, a protein extract of PYL4-Nluc was added, and the mixture was incubated for 2 h at 4^{o}C. Finally, precipitates were detected using an anti-Luc antibody.

Antibodies resources

The antibodies anti-Myc and RFP were bought from Easy Bio System Inc.; anti-Luc was from Sigma; anti-P4D1 and anti-HA were bought from Santa Cruz Biotechnology; anti-FK1 was from Millipore, anti-ABI5 is from Abcam, K48 and K63 are from Cell Signaling; and anti-Ub and PYL4 are the stock of our own lab.

ACCESSION NUMBERS

Arabidopsis Genome Initiative locus identifiers for the genes mentioned in this article are as follows: *VPS23A* (AT3G12400), *PYR1* (AT4G17870), *PYL1* (AT5G46790), *PYL2* (AT2G26040), *PYL3* (AT1G73000), *PYL4* (AT2G38310), *PYL5* (AT5G05440), *PYL6*

(AT2G40330), *PYL7* (AT4G01026), *PYL8* (AT5G53160), *PYL9* (AT1G01360), *PYL10* (AT4G27920), *PYL11* (AT5G45860), *PYL12* (AT5G45870), *PYL13* (AT4G18620), *OST1* (AT4G33950), *ABI4* (AT2G40220), *ABI5* (AT2G36270), *ABI1* (AT4G26080), *HAB1* (AT1G72770), *PAG* (AT2G27020), *ACTIN 1* (AT2G37620), *ACTIN 7* (AT5G09810).

AUTHOR CONTRIBUTIONS

Q.X. and F.Y. designed the experiments and wrote the paper. F.Y. performed the experiments. L.L. and M.T. analyzed the phenotype of *vps23a* mutant. Q.L. and M.T. prepared the vector constructs. X.C. prepared some plant materials. Y.W. provided the technique support. Y.D. and S.Y. assayed the OST1 activity. B.B and P.R provide HA-PYL4 transgenic plants and mCherry-VPS23A vector.

ACKNOWLEDGEMENTS

This research was supported by grant 2016YFA0500500 from the National Basic Research Program of China and NSFC 31571441 from the National Science Foundation of China. We thank the Arabidopsis Biological Resource Center (ABRC) at Ohio State University for providing the T-DNA insertion lines.

REFERENCES

Antoni, R., Gonzalez-Guzman, M., Rodriguez, L., Peirats-Llobet, M., Pizzio, G.A., Fernandez, M.A., De Winne, N., De Jaeger, G., Dietrich, D., Bennett, M.J., et al. (2013). PYRABACTIN RESISTANCE1-LIKE8 plays an important role for the regulation of abscisic acid signaling in root. Plant Physiol. **161**, 931-941.

Armstrong, F., Leung, J., Grabov, A., Brearley, J., Giraudat, J., and Blatt, M.R. (1995). Sensitivity to abscisic-acid of guard-cell K+ channels is suppressed by *abi1-1*, a mutant Arabidopsis gene encoding a putative protein phosphatase. Proc. Natl. Acad. Sci. U S A **92**, 9520-9524.

Babst, M., Odorizzi, G., Estepa, E.J., and Emr, S.D. (2000). Mammalian tumor susceptibility gene 101 (TSG101) and the yeast homologue, Vps23p, both function in late endosomal

trafficking. Traffic **1**, 248-258.

Barberon, M., Dubeaux, G., Kolb, C., Isono, E., Zelazny, E., and Vert, G. (2014). Polarization of IRON-REGULATED TRANSPORTER 1 (IRT1) to the plant-soil interface plays crucial role in metal homeostasis. Proc. Natl. Acad. Sci. U S A **111**, 8293-8298.

Barberon, M., Zelazny, E., Robert, S., Conejero, G., Curie, C., Friml, J., and Vert, G. (2011). Monoubiquitin-dependent endocytosis of the IRON-REGULATED TRANSPORTER 1 (IRT1) transporter controls iron uptake in plants. Proc. Natl. Acad. Sci. U S A **108**, E450-E458.

Bassham, D.C. (2007). Plant autophagy-more than a starvation response. Curr. Opin. Plant Biol. **10**, 587-593.

Bayle, V., Arrighi, J.F., Creff, A., Nespoulous, C., Vialaret, J., Rossignol, M., Gonzalez, E., Paz-Ares, J., and Nussaume, L. (2011). *Arabidopsis thaliana* high-affinity phosphate transporters exhibit multiple levels of posttranslational regulation. Plant Cell **23**, 1523-1535.

Bilodeau, P.S., Urbanowski, J.L., Winistorfer, S.C., and Piper, R.C. (2002). The Vps27p-Hse1p complex binds ubiquitin and mediates endosomal protein sorting. Nature Cell Biol. **4**, 534-539.

Belda-Palazon, B., Rodriguez, L., Fernandez, M.A., Castillo, M.C., Anderson, E.A., Gao, C., Gonzalez-Guzman, M., Peirats-Llobet, M., Zhao, Q., De Winne, N., et al. (2016). FYVE1/FREE1 interacts with the PYL4 ABA receptor and mediates its delivery to the vacuolar degradation pathway. Plant Cell DOI: 10.1105/tpc.16.00178.

Bilodeau, P.S., Winistorfer, S.C., Kearney, W.R., Robertson, A.D., and Piper, R.C. (2003). Vps27-Hse1 and ESCRT-I complexes cooperate to increase efficiency of sorting ubiquitinated proteins at the endosome. J. Cell Biol. **163**, 237-243.

Bossi, F., Cordoba, E., Dupre, P., Mendoza, M.S., Roman, C.S., and Leon, P. (2009). The Arabidopsis ABA-INSENSITIVE (ABI) 4 factor acts as a central transcription activator of the expression of its own gene, and for the induction of *ABI5* and *SBE2.2* genes during sugar signaling. Plant J. **59**, 359-374.

Bueso, E., Rodriguez, L., Lorenzo-Orts, L., Gonzalez-Guzman, M., Sayas, E., Munoz-Bertomeu, J., Ibanez, C., Serrano, R., and Rodriguez, P.L. (2014). The single-subunit RING-type E3 ubiquitin ligase RSL1 targets PYL4 and PYR1 ABA receptors in plasma

membrane to modulate abscisic acid signaling. Plant J. **80**, 1057-1071.

Clague, M.J., and Urbe, S. (2006). Endocytosis: the DUB version. Trends Cell Biol. **16**, 551-559.

Clough, S.J., and Bent, A.F. (1998). Floral dip: a simplified method for Agrobacterium-mediated transformation of *Arabidopsis thaliana*. Plant J. **16**, 735-743.

Ding, Y.L., Li, H., Zhang, X.Y., Xie, Q., Gong, Z.Z., and Yang, S.H. (2015). OST1 kinase modulates freezing tolerance by enhancing ICE1 stability in Arabidopsis. Dev. Cell **32**, 278-289.

Fujii, H., Verslues, P.E., and Zhu, J.K. (2007). Identification of two protein kinases required for abscisic acid regulation of seed germination, root growth, and gene expression in Arabidopsis. Plant Cell **19**, 485-494.

Furihata, T., Maruyama, K., Fujita, Y., Umezawa, T., Yoshida, R., Shinozaki, K., and Yamaguchi-Shinozaki, K. (2006). Abscisic acid-dependent multisite phosphorylation regulates the activity of a transcription activator AREB1. Proc. Natl. Acad. Sci. U S A **103**, 1988-1993.

Gao, C.J., Luo, M., Zhao, Q., Yang, R.Z., Cui, Y., Zeng, Y.L., Xia, J., and Jiang, L.W. (2014). A unique plant ESCRT component, FREE1, regulates multivesicular body protein sorting and plant growth. Curr. Biol. **24**, 2556-2563.

Gao, C., Zhuang, X., Cui, Y., Fu, X., He, Y., Zhao, Q., Zeng, Y., Shen, J., Luo, M., and Jiang, L. (2015). Dual roles of an Arabidopsis ESCRT component FREE1 in regulating vacuolar protein transport and autophagic degradation. Proc. Natl. Acad. Sci. U S A **112**, 1886-1891.

Geldner, N., Friml, J., Stierhof, Y.D., Jurgens, G., and Palme, K. (2001). Auxin transport inhibitors block PIN1 cycling and vesicle traficking. Nature **413**, 425-428.

Haas, T.J., Sliwinski, M.K., Martinez, D.E., Preuss, M., Ebine, K., Ueda, T., Nielsen, E., Odorizzi, G., and Otegui, M.S. (2007). The Arabidopsis AAA ATPase SKD1 is involved in multivesicular endosome function and interacts with its positive regulator LYST-INTERACTING PROTEIN5. Plant Cell **19**, 1295-1312.

Hao, Q., Yin, P., Li, W., Wang, L., Yan, C., Lin, Z., Wu, J.Z., Wang, J., Yan, S.F., and Yan, N. (2011). The molecular basis of ABA-independent inhibition of PP2Cs by a subclass of PYL proteins. Mol. Cell **42**, 662-672.

Henne, W.M., Stenmark, H., and Emr, S.D. (2013). Molecular mechanisms of the membrane sculpting ESCRT pathway. Cold Spring Harb. Perspect. Biol. **5**.

Hurley, J.H., and Emr, S.D. (2006). The ESCRT complexes: structure and mechanism of a membrane-trafficking network. Annu. Rev. Biophys. Biomol. Struct. **35**, 277-298.

Irigoyen, M.L., Iniesto, E., Rodriguez, L., Puga, M.I., Yanagawa, Y., Pick, E., Strickland, E., Paz-Ares, J., Wei, N., De Jaeger, G., et al. (2014). Targeted degradation of abscisic acid receptors is mediated by the ubiquitin ligase substrate adaptor DDA1 in Arabidopsis. Plant Cell **26**, 712-728.

Jiang, Y., Ou, Y., and Cheng, X. (2013). Role of TSG101 in cancer. Front. Biosci. (Landmark Ed) **18**, 279-288.

Kalinowska, K., Nagel, M.K., Goodman, K., Cuyas, L., Anzenberger, F., Alkofer, A., Paz-Ares, J., Braun, P., Rubio, V., Otegui, M.S., et al. (2015). Arabidopsis ALIX is required for the endosomal localization of the deubiquitinating enzyme AMSH3. Proc. Natl. Acad. Sci. U S A **112**, e5543-5551.

Kasai, K., Takano, J., Miwa, K., Toyoda, A., and Fujiwara, T. (2011). High Boron-induced ubiquitination regulates vacuolar sorting of the BOR1 borate transporter in Arabidopsis thaliana. J. Biol. Chem. **286**, 6175-6183.

Katzmann, D.J., Stefan, C.J., Babst, M., and Emr, S.D. (2003). Vps27 recruits ESCRT machinery to endosomes during MVB sorting. J. Cell Biol. **162**, 413-423.

Kleine-Vehn, J., Dhonukshe, P., Swarup, R., Bennett, M., and Friml, J. (2006). Subcellular trafficking of the Arabidopsis auxin influx carrier AUX1 uses a novel pathway distinct from PIN1. Plant Cell **18**, 3171-3181.

Kleine-Vehn, J., Leitner, J., Zwiewka, M., Sauer, M., Abas, L., Luschnig, C., and Friml, J. (2008). Differential degradation of PIN2 auxin efflux carrier by retromer-dependent vacuolar targeting. Proc. Natl. Acad. Sci. U S A **105**, 17812-17817.

Lauwers, E., Jacob, C., and Andre, B. (2009). K63-linked ubiquitin chains as a specific signal for protein sorting into the multivesicular body pathway. J. Cell Biol. **185**, 493-502.

Leitner, J., Petrasek, J., Tomanov, K., Retzer, K., Parezova, M., Korbei, B., Bachmair, A., Zazimalova, E., and Luschnig, C. (2012). Lysine^{63}-linked ubiquitylation of PIN2 auxin carrier protein governs hormonally controlled adaptation of Arabidopsis root growth. Proc. Natl.

Acad. Sci. U S A **109**, 8322-8327.

Liu, L.J., Zhang, Y.Y., Tang, S.Y., Zhao, Q.Z., Zhang, Z.H., Zhang, H.W., Dong, L., Guo, H.S., and Xie, Q. (2010). An efficient system to detect protein ubiquitination by agroinfiltration in *Nicotiana benthamiana*. Plant J. **61**, 893-903.

Li, Y., Kane, T., Tipper, C., Spatrick, P., and Jenness, D.D. (1999). Yeast mutants affecting possible quality control of plasma membrane proteins. Mol. Cell Biol. **19**, 3588-3599.

Lu, Q., Hope, L.W., Brasch, M., Reinhard, C., and Cohen, S.N. (2003). TSG101 interaction with HRS mediates endosomal trafficking and receptor down-regulation. Proc. Natl. Acad. Sci. U S A **100**, 7626-7631.

Ma, Y., Szostkiewicz, I., Korte, A., Moes, D., Yang, Y., Christmann, A., and Grill, E. (2009). Regulators of PP2C phosphatase activity function as abscisic acid sensors. Science **324**, 1064-1068.

Martins, S., Dohmann, E.M., Cayrel, A., Johnson, A., Fischer, W., Pojer, F., Satiat-Jeunemaitre, B., Jaillais, Y., Chory, J., Geldner, N., et al. (2015). Internalization and vacuolar targeting of the brassinosteroid hormone receptor BRI1 are regulated by ubiquitination. Nat. Commun. **6**, 6151.

Mukhopadhyay, D., and Riezman, H. (2007). Proteasome-independent functions of ubiquitin in endocytosis and signaling. Science **315**, 201-205.

Mustilli, A.C., Merlot, S., Vavasseur, A., Fenzi, F., and Giraudat, J. (2002). Arabidopsis OST1 protein kinase mediates the regulation of stomatal aperture by abscisic acid and acts upstream of reactive oxygen species production. Plant Cell **14**, 3089-3099.

Park, S.Y., Fung, P., Nishimura, N., Jensen, D.R., Fujii, H., Zhao, Y., Lumba, S., Santiago, J., Rodrigues, A., Chow, T.F., et al. (2009). Abscisic acid inhibits type 2C protein phosphatases via the PYR/PYL family of START proteins. Science **324**, 1068-1071.

Raghavendra, A.S., Gonugunta, V.K., Christmann, A., and Grill, E. (2010). ABA perception and signalling. Trends Plant Sci. **15**, 395-401.

Reyes, F.C., Buono, R., and Otegui, M.S. (2011). Plant endosomal trafficking pathways. Curr. Opin. Plant Biol. **14**, 666-673.

Robinson, D.G., Jiang, L.W., and Schumacher, K. (2008). The endosomal system of plants: charting new and familiar territories. Plant Physiol. **147**, 1482-1492.

Rodriguez, L., Gonzalez-Guzman, M., Diaz, M., Rodrigues, A., Izquierdo-Garcia, A.C., Peirats-Llobet, M., Fernandez, M.A., Antoni, R., Fernandez, D., Marquez, J.A., *et al.* (2014). C2-domain abscisic acid-related proteins mediate the interaction of PYR/PYL/RCAR abscisic acid receptors with the plasma membrane and regulate abscisic acid sensitivity in Arabidopsis. Plant Cell **26**, 4802-4820.

Saez, A., Robert, N., Maktabi, M.H., Schroeder, J.I., Serrano, R., and Rodriguez, P.L. (2006). Enhancement of abscisic acid sensitivity and reduction of water consumption in Arabidopsis by combined inactivation of the protein phosphatases type 2C ABI1 and HAB1. Plant Physiol. **141**, 1389-1399.

Scott, A., Chung, H.Y., Gonciarz-Swiatek, M., Hill, G.C., Whitby, F.G., Gaspar, J., Holton, J.M., Viswanathan, R., Ghaffarian, S., Hill, C.P., et al. (2005). Structural and mechanistic studies of VPS4 proteins. EMBO J. **24**, 3658-3669.

Shields, S.B., and Piper, R.C. (2011). How ubiquitin functions with ESCRTs. Traffic **12**, 1306-1317.

Slagsvold, T., Pattni, K., Malerod, L., and Stenmark, H. (2006). Endosomal and non-endosomal functions of ESCRT proteins. Trends Cell Biol. **16**, 317-326.

Spallek, T., Beck, M., Ben Khaled, S., Salomon, S., Bourdais, G., Schellmann, S., and Robatzek, S. (2013). ESCRT-I mediates FLS2 endosomal sorting and plant immunity. Plos Genet. **9**, e1004035.

Spitzer, C., Reyes, F.C., Buono, R., Sliwinski, M.K., Haas, T.J., and Otegui, M.S. (2009). The ESCRT-Related CHMP1A and B proteins mediate multivesicular body sorting of auxin carriers in Arabidopsis and are required for plant development. Plant Cell **21**, 749-766.

Spitzer, C., Schellmann, S., Sabovljevic, A., Shahriari, M., Keshavaiah, C., Bechtold, N., Herzog, M., Muller, S., Hanisch, F.G., and Hulskamp, M. (2006). The Arabidopsis *elch* mutant reveals functions of an ESCRT component in cytokinesis. Development **133**, 4679-4689.

Tomanov, K., Luschnig, C., and Bachmair, A. (2014). Ubiquitin Lys 63-chains second-most abundant, but poorly understood in plants. Front. Plant Sci. **5**, 15.

Traub, L.M., and Lukacs, G.L. (2007). Decoding ubiquitin sorting signals for clathrin-dependent endocytosis by CLASPs. J. Cell Sci. **120**, 543-553.

Valencia, J.P., Goodman, K., and Otegui, M.S. (2016). Endocytosis and endosomal trafficking in plants. Annu. Rev. Plant Biol. **67**, 309-335.

Vlad, F., Rubio, S., Rodrigues, A., Sirichandra, C., Belin, C., Robert, N., Leung, J., Rodriguez, P.L., Lauriere, C., and Merlot, S. (2009). Protein phosphatases 2C regulate the activation of the SNF1-related kinase OST1 by abscisic acid in Arabidopsis. Plant Cell **21**, 3170-3184.

Wang, F., Yang, Y., Wang, Z., Zhou, J., Fan, B., and Chen, Z. (2015). A critical role of Lyst-Interacting Protein5, a positive regulator of multivesicular body biogenesis, in plant responses to heat and salt stresses. Plant Physiol. **169**, 497-511.

Xia, Z.L., Huo, Y.J., Wei, Y.Y., Chen, Q.S., Xu, Z.W., and Zhang, W. (2016). The Arabidopsis LYST INTERACTING PROTEIN 5 acts in regulating abscisic acid signaling and drought response. Front. Plant Sci. **7**, 758.

Xie, Q., Guo, H.S., Dallman, G., Fang, S.Y., Weissman, A.M., and Chua, N.H. (2002). SINAT5 promotes ubiquitin-related degradation of NAC1 to attenuate auxin signals. Nature **419**, 167-170.

Xie, Q., Sanz-Burgos, A.P., Guo, H.S., Garcia, J.A., and Gutierrez, C. (1999). GRAB proteins, novel members of the NAC domain family, isolated by their interaction with a geminivirus protein. Plant Mol. Biol. **39**, 647-656.

Yu, F., Wu, Y.R., and Xie, Q. (2015). Precise protein post-translational modifications modulate ABI5 activity. Trends Plant Sci. **20**, 569-575.

Yu, F., Wu, Y., and Xie, Q. (2016). Ubiquitin-proteasome system in aba signaling: from perception to action. Mol. Plant **9**, 21-33.

FIGURE LEGENDS

Figure 1. The *vps23a* mutant is more sensitive to ABA than wild-type Col-0.

(A) *vps23a* is sensitive to ABA in terms of cotyledon greening and root growth. Seeds of Col-0, *vps23a* and P_{VPS23A}-*VPS23A* (*vps23a*) 3.3 and 4.6 lines were germinated on ½ MS medium containing 0, 0.3 and 0.5 µM ABA. Representative plants were photographed after one week. Scale bar, 0.5 cm.

(B) Statistical analysis of root length measured in the Col-0 wide type, *vps23a*, and P_{VPS23A}-*VPS23A* (*vps23a*) 3.3 and 4.6 lines that are shown in Figure 1A. Three replicates were conducted. Values are means ± SD (n=30). Asterisks indicate statistical differences ($P < 0.05$) according to Tukey's test, two asterisks indicate $P<0.01$, and three asterisks indicates $P<0.001$.

Figure 2. In-gel kinase activity assay of OST1 and analysis of ABA-responsive gene expression in the *vps23a* mutant.

(A) OST1 activity is enhanced in the *vps23a* mutant. Ten-day-old seedlings were treated with or without 50 μM ABA for 30 min. Total proteins were separated by 10% SDS-PAGE containing OST1 substrate GST1-ΔABF2. The protein kinase assay buffer contained [γ-32P]ATP. Radioactivity is shown at the top. The triangle indicates the phosphorylated signal. Asterisks indicate nonspecific bands. Ponceau S-stained ribulose-1,5-bisphosphate carboxylase/oxygenase (Rubisco) was used as an internal control (bottom).

(B) qRT-PCR assay to determine the transcriptional level of *ABI4*. Seeds of Col-0 and *vps23a* were sown on ½ MS medium containing 0 or 0.5 μM ABA. After 7 days, the seedlings were collected for RNA extraction and qRT-PCR assay. Three replicates were conducted. Asterisks indicate statistical differences ($P < 0.05$) according to Tukey's test.

(C) qRT-PCR assay to determine the transcriptional level of *ABI5*. The treatment and analysis are the same as those described in (B).). Asterisks indicate statistical differences ($P < 0.05$) according to Tukey's test. Three replicates were conducted.

(D) ABI5 protein level is increased in the *vps23a* mutant in response to ABA or NaCl treatment. Seeds of Col-0 and *vps23a* were sown on ½ MS medium containing 0 or 0.5 μM ABA or 125 mM NaCl. After 4 days, Western blot analysis was conducted using an anti-ABI5 antibody. Anti-PAG1 (20S proteasome α-subunit G1) was used as a loading control.

Figure 3. The epistatic relation between *VPS23A* and *PYR/PYL/RCAR*.

(A) *VPS23A* acts upstream of *ABI4* and *ABI5*. Seeds of Col-0, *vps23a*, *abi4-T*, *vps23a abi4-T*, Ws, *abi5-1* and *vps23a abi5-1* were germinated on ½ MS medium containing 0 or 0.3 μM ABA. After approximately 10 days, the seedlings were photographed. Scale bar, 1 cm.

(B) The epistatic relations between *VPS23A* and *ABI1* or *PYR/PYL/RCAR*. Seeds of Col-0, *vps23a*, *abi1-1*, *abi1-1 vps23a*, L*er*, *pyr1 pyl1/2/4* and *pyr1 pyl1/2/4 vps23a* were germinated on ½ MS medium in the absence or presence of ABA. After approximately 10 days, the seedlings were photographed. Scale bar, 1 cm.

Figure 4. Localization of PYR1/PYL4 in endosomal compartments.

(A) VPS23A partially localizes on both early and late endosomes. SCAMP1-RFP, MANI-RFP and ARA7-RFP are early endosome, *trans*-Golgi network (TGN) and late endosome markers, respectively. Transient co-expression of GFP-VPS23A and SCAMP1-RFP/MANI-RFP/ARA7-RFP were performed in tobacco leaves by agroinfiltration. After 3 days, the resulting fluorescence was observed by Confocal Laser Scanning Microscopy (CLSM). The excitation wavelength was 488 nm and 563 nm for the GFP and mCherry signals, respectively. The yellow signal in the third lane represents merged GFP and RFP signals. Scale bars, 5 μm.

(B) PYR1/PYL4 partially localizes on the early endosome and TGN. Scale bars, 10 μm.

(C) PYR1/PYL4 partially localizes on the late endosome. Treatment with the inhibitor Wortmannin (WM) led more globular fluorescent signals, and the merged GFP signal of PYR1/PYL4 and the RFP signal of ARA7 after WM treatment was more intense than that observed without WM treatment. Scale bars, 10 μm.

(D) PYR1/PYL4 co-localizes with VPS23A. Co-expression of PYR1/PYL4-GFP and mCherry-VPS23A in tobacco leaves was performed by agroinfiltration. A time-course showed the co-migration of PYR1/PYL4-GFP with mCherry-VPS23A in endosome compartments.

Figure 5. VPS23A interacts with PYL4.

(A) VPS23A interacts with PYL4 *in vitro* according to a Co-IP assay. GFP and GFP-VPS23A were immunoprecipitated with anti-GFP antibody, which was coated on magnetic beads; then, an equal amount of PYL4-Nluc was added, and the mixture was incubated for another 2 h at

4°C. Anti-GFP and anti-Luc antibodies were used to separately detect GFP/GFP-VPS23A and PYL4-Nluc. PYL4-Nluc co-immunoprecipitated with GFP-VPS23A but not with the GFP control. GFP and GFP-VPS23A are indicated by open arrowheads. PYL4-Nluc is indicated by a dark arrowhead. The asterisk indicates a degraded form of GFP-VPS23A.

(B) VPS23A interacts with PYL4 *in vivo* as shown by luciferase complementation imaging (LCI). VPS23A fused to the C-terminal fragment of luciferase (Cluc) was co-expressed with PYL4 fused to the N-terminal fragment of luciferase (Nluc) by agroinfiltration in tobacco leaves; Nluc and Cluc were used as negative controls. Reconstituted luciferase activity was detected after 4 days.

(C) VPS23A interacts with the K63-linked ubiquitin forms of PYL4. *E. coli*-expressed GST and GST-VPS23A proteins were incubated with plant expressed PYL4-Nluc protein in a pull-down assay. After incubation for 2 h at 4°C and three time washes, an immunoblot assay was performed using anti-Luc, anti-Ub and anti-K63-Ub antibodies.

(D) VPS23A binds K63-linked ubiquitin. *E. coli*-expressed GST and GST-VPS23A proteins were incubated with K63-linked ubiquitin for 2 h at 4°C, after three time washes, anti-Ub was utilized to detect the precipitated K63-linked ubiquitin. Ponceau S-stained GST and GST-VPS23A were shown.

Figure 6. VPS23A affects the subcellular localization of PYR1.

(A) VPS23A affects vacuole biogenesis. The upper BCECF-AM staining shows tubular-like structures in the vacuoles of the *vps23a* mutant. The bottom image indicates 3D surface renderings of vacuoles of several representative root epidermal cells of 2-day-old wild-type and *vps23a* mutant plants. Scale bars, 5 µm.

(B) VPS23A affects the subcellular localization of PYR1. Confocal images of root epidermal cells from 10-day-old wild-type (Col-0) and *vps23a* mutant plants over-expressing PYR1-GFP are shown. Membrane-associated FM4-64 staining was performed as shown by the red channels. The yellow signal represents an overlay of the GFP and RFP channels. The arrows indicate the increase in vesicle-like compartments in the *vps23a* mutant. Scale bars, 10 µm.

Figure 7. VPS23A promotes the degradation of PYL4.

(A) PYL4 can be degraded through the lysosomal pathway. Approximately 10-day-old transgenic plants of HA-PYL4 were treated with cycloheximide and with/without E64D. Samples were collected at 0, 2, 4 and 6 hours. HA-PYL4 was detected using an anti-HA antibody. PAG was used as the internal control.

(B) VPS23A facilitates the degradation of PYL4. GFP- and GFP-VPS23A-transformed *A. tumefaciens* plants were co-infiltrated with same amount of PYL4-Nluc construct-transformed *A. tumefaciens* plants, and RFP was used as an internal expression control. Total RNA was extracted from the injected tobacco leaves, and RT-PCR assays of *PYL4* were carried out to determine the transcription level of *PYL4*.

(C) VPS23A facilitates the degradation of PYL4 *in vitro*. Equal amounts of transiently expressed GFP-PYL4 protein were mixed with different amounts of Myc-VPS23A and incubated at 22^{o}C for 2 h. Anti-GFP and anti-Myc antibodies were utilized in immunoblot assays. Ponceau S-stained rubisco was used as the loading control.

(D) HA-PYL4 degradation is alleviated in the *vps23a* mutant. Seedlings of Col-0 and *vps23a* mutant plants overexpressing HA-PYL4 were pretreated with ½ MS medium overnight and then incubated with 50 μM CHX. Samples were collected at 0, 2, 4 and 8 h and subjected to immunoblot assays. Anti-PAG1 was used as the internal control.

(E) PYL4 accumulates in *vps23a* compared with Col-0. Seeds of Col-0 and *vps23a* were sown on ½ MS medium without or with 0.3 μM ABA, two days later, the seedlings were transferred to darkness condition for 6 days. Total proteins were extracted and subjected to immunoblot assays. Anti-PAG1 was used as the internal control.

A

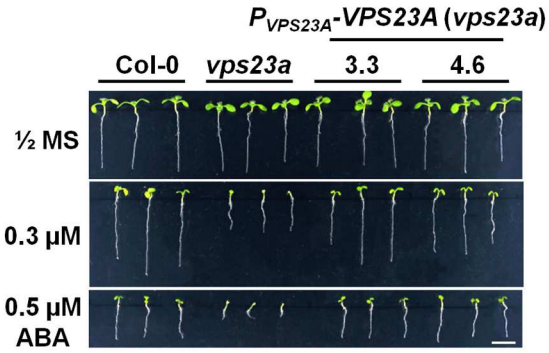

B

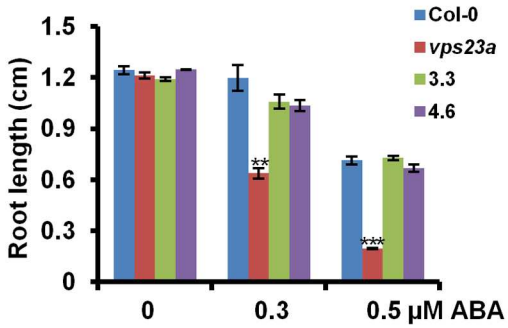

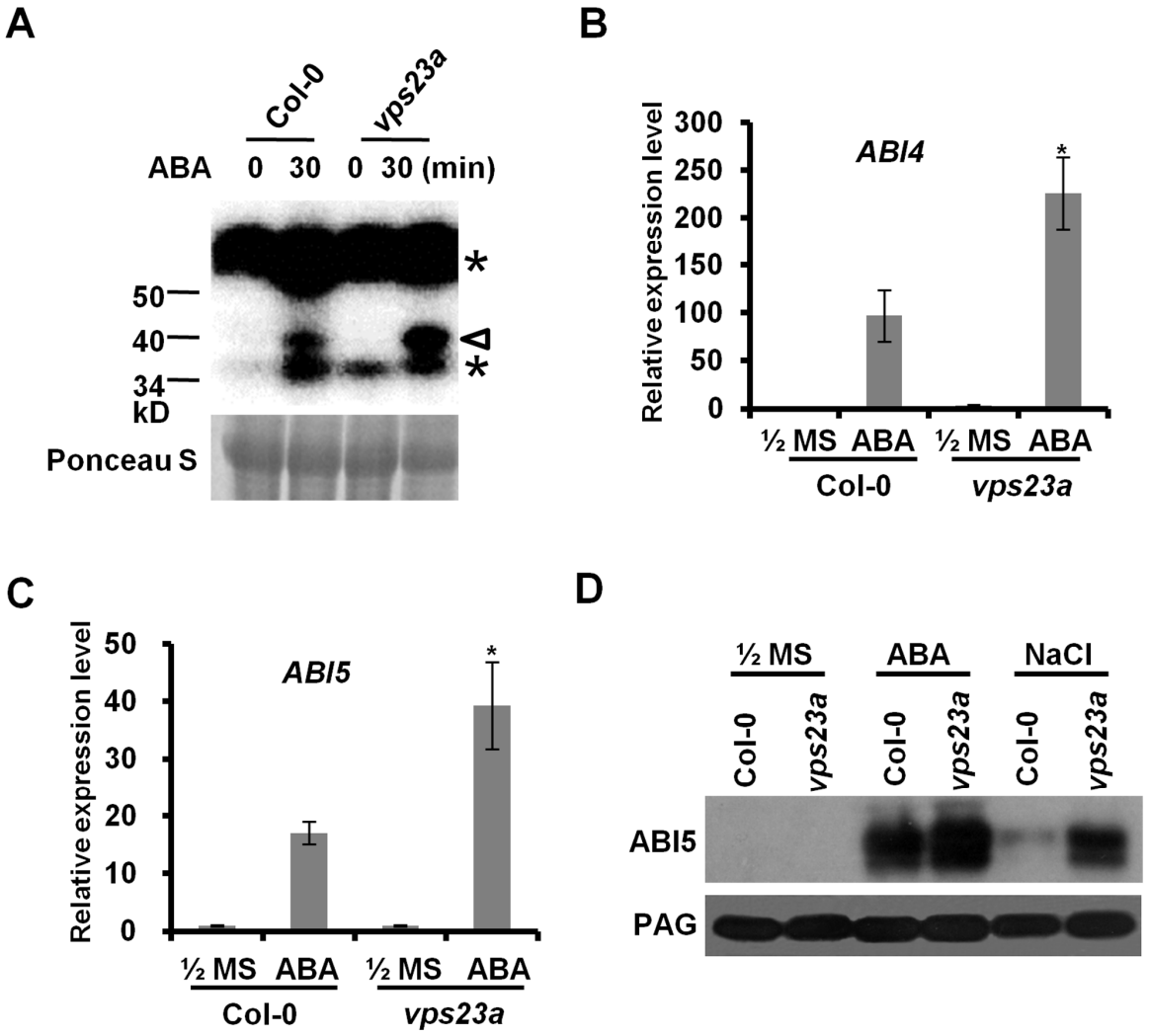
A
Col-0
vps23a
ABA 0 30 0 30 (min)
50
40
34
kD
*
*Δ
Ponceau S
B
Relative expression level
ABI4
300
250
200
150
100
50
0
*
½ MS ABA ½ MS ABA
Col-0
vps23a
C
Relative expression level
ABI5
50
40
30
20
10
0
*
½ MS ABA ½ MS ABA
Col-0
vps23a
D
½ MS
ABA
NaCl
Col-0
vps23a
Col-0
vps23a
Col-0
vps23a
ABI5
PAG

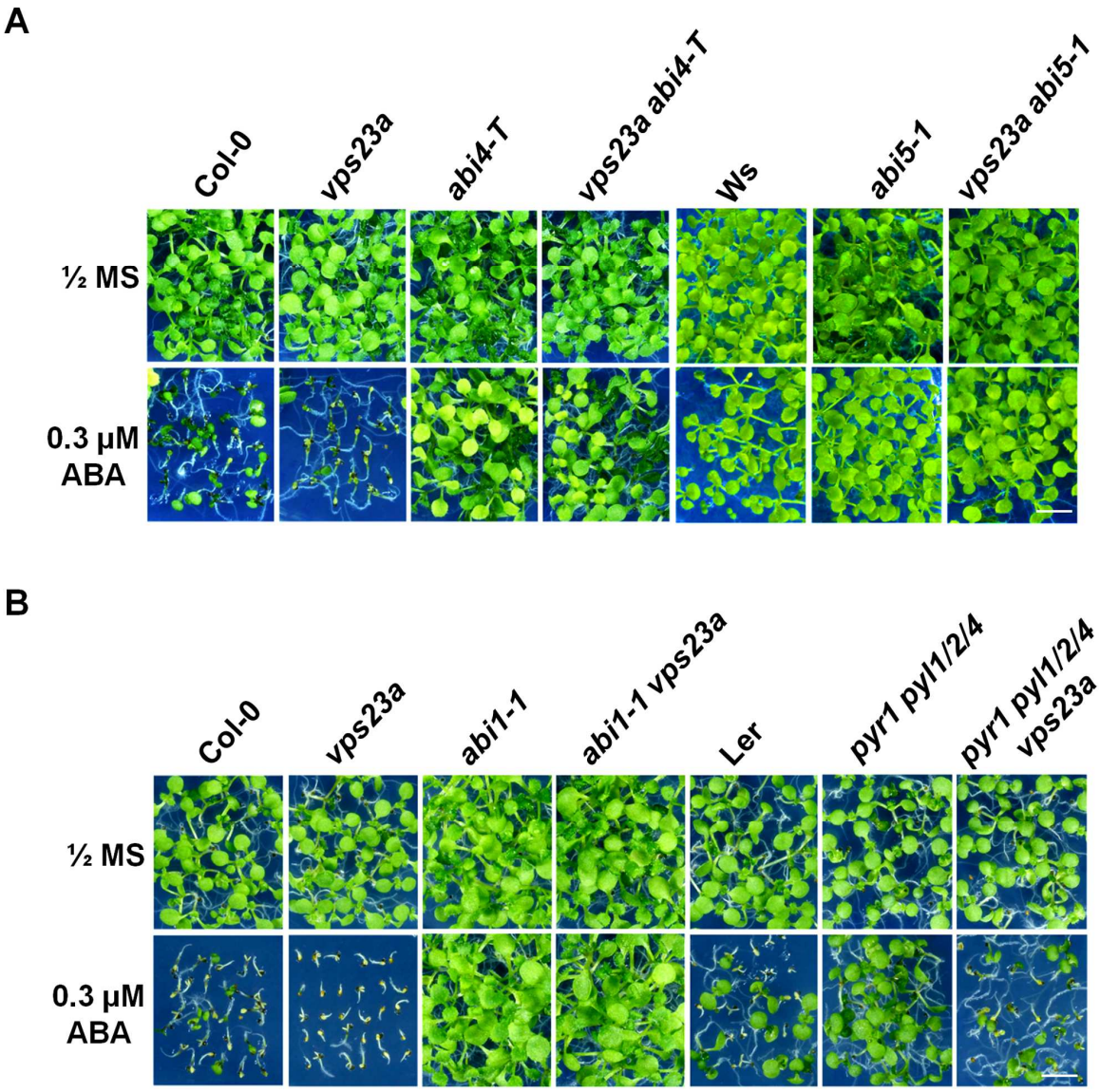
A
Col-0
vps23a
abi4-T
vps23a abi4-T
Ws
abi5-1
vps23a abi5-1
½ MS
0.3 µM ABA
B
Col-0
vps23a
abi1-1
abi1-1 vps23a
Ler
pyr1 pyl1/2/4
pyr1 pyl1/2/4 vps23a
½ MS
0.3 µM ABA

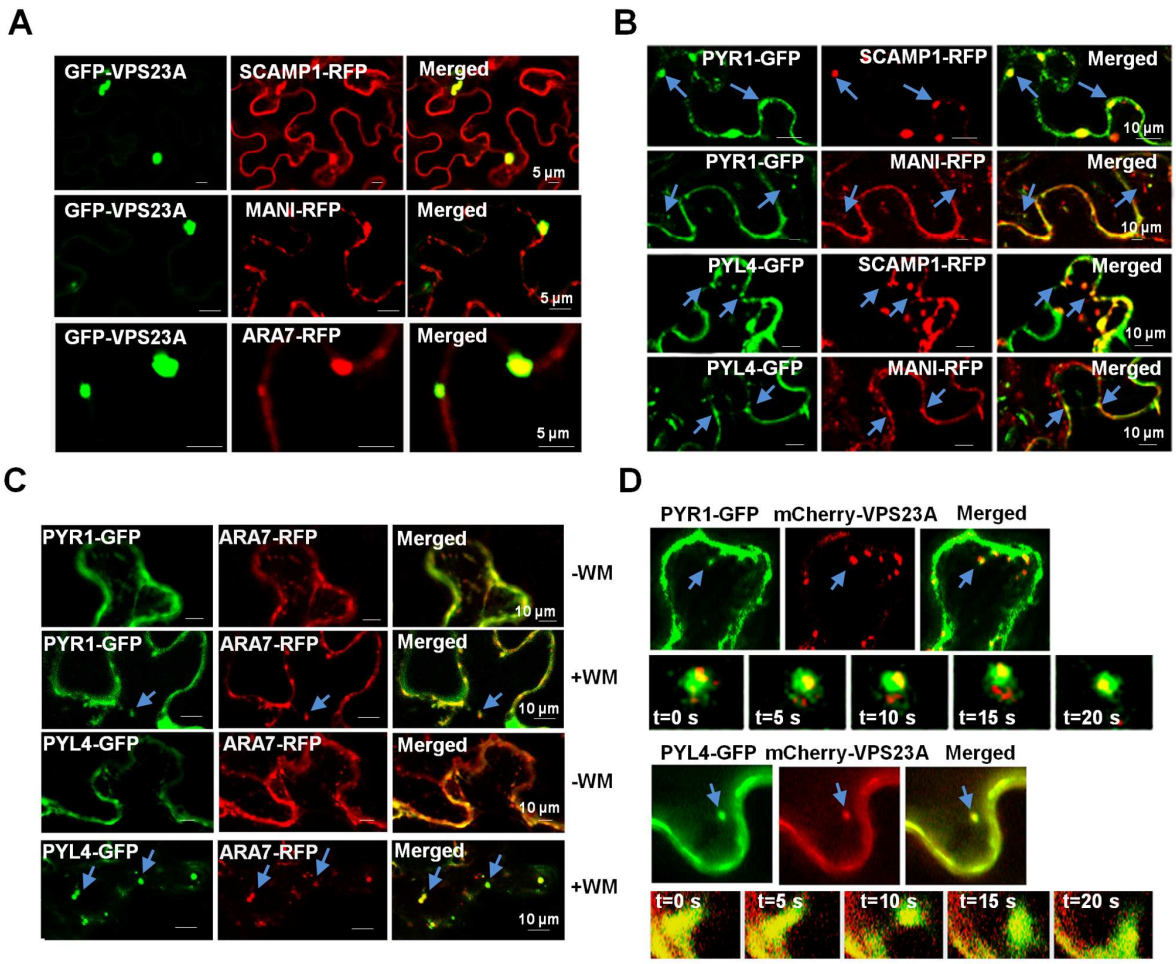
A
GFP-VPS23A
SCAMP1-RFP
Merged
5 μm
GFP-VPS23A
MANI-RFP
Merged
5 μm
GFP-VPS23A
ARA7-RFP
Merged
5 μm
B
PYR1-GFP
SCAMP1-RFP
Merged
10 μm
PYR1-GFP
MANI-RFP
Merged
10 μm
PYL4-GFP
SCAMP1-RFP
Merged
10 μm
PYL4-GFP
MANI-RFP
Merged
10 μm
C
PYR1-GFP
ARA7-RFP
Merged
10 μm
-WM
PYR1-GFP
ARA7-RFP
Merged
10 μm
+WM
PYL4-GFP
ARA7-RFP
Merged
10 μm
-WM
PYL4-GFP
ARA7-RFP
Merged
10 μm
+WM
D
PYR1-GFP mCherry-VPS23A Merged
t=0 s
t=5 s
t=10 s
t=15 s
t=20 s
PYL4-GFP mCherry-VPS23A Merged
t=0 s
t=5 s
t=10 s
t=15 s
t=20 s

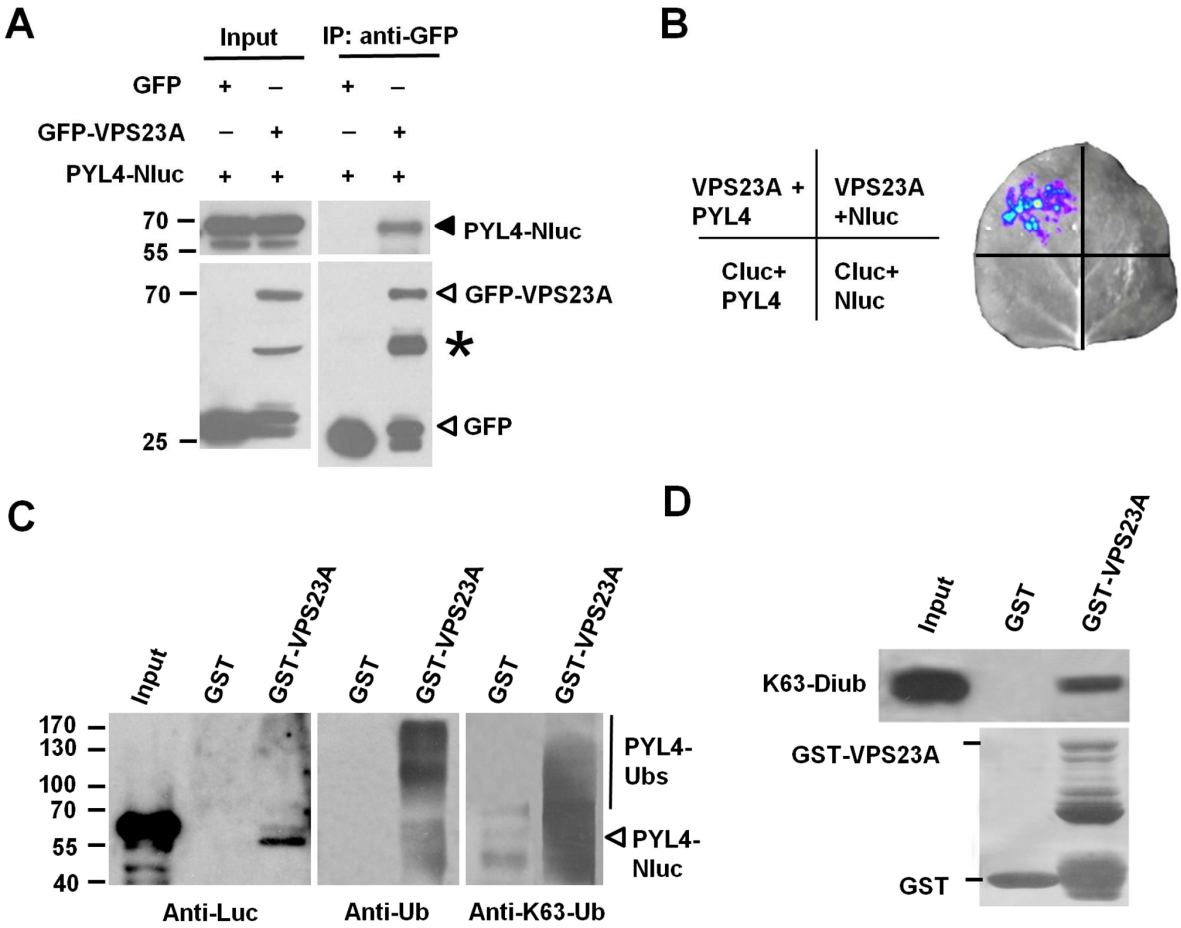
A
Input
IP: anti-GFP
GFP + – + –
GFP-VPS23A – + – +
PYL4-Nluc + + + +
70
55
70
25
PYL4-Nluc
GFP-VPS23A
*
GFP
B
VPS23A + PYL4
VPS23A +Nluc
Cluc+ PYL4
Cluc+ Nluc
C
Input
GST
GST-VPS23A
GST
GST-VPS23A
GST
GST-VPS23A
170
130
100
70
55
40
PYL4-Ubs
PYL4-Nluc
Anti-Luc
Anti-Ub
Anti-K63-Ub
D
Input
GST
GST-VPS23A
K63-Diub
GST-VPS23A
GST

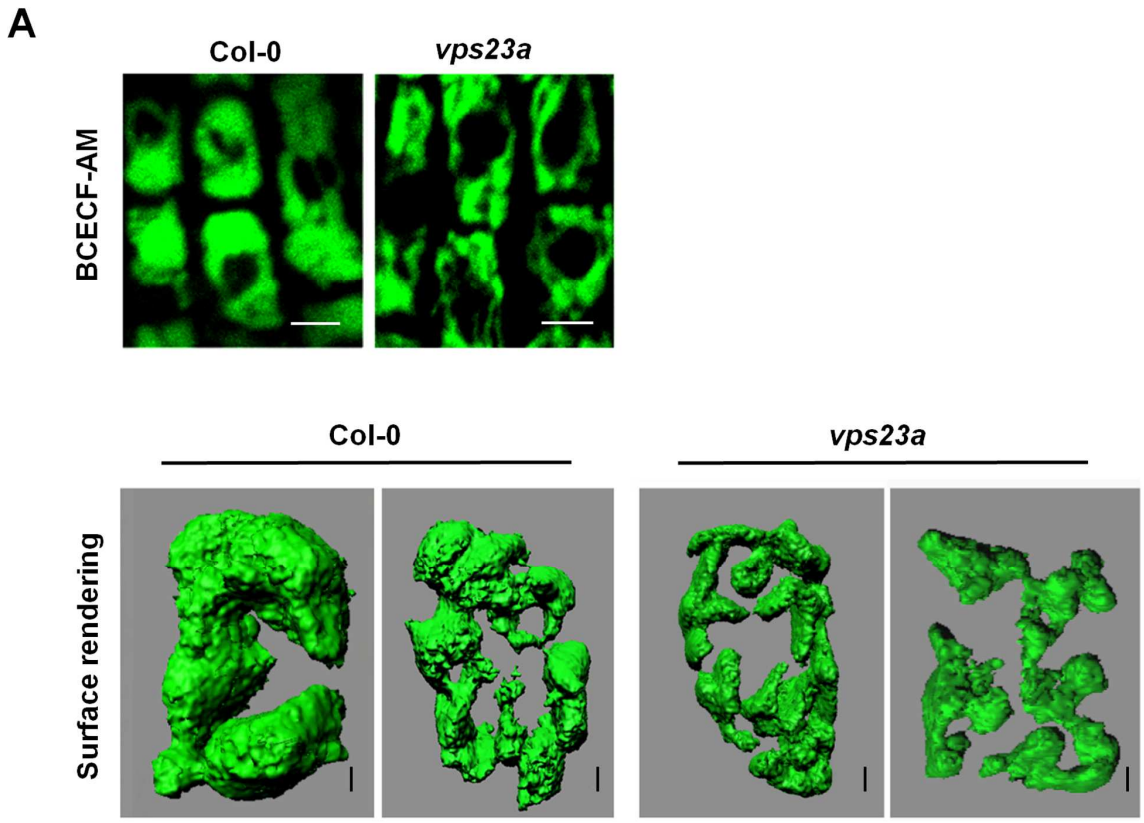
A
Col-0
vps23a
BCECF-AM
Col-0
vps23a
Surface rendering
B
PYR1-GFP
Col-0
FM4-64
Merge
PYR1-GFP
vps23a
FM4-64
Merge